
SHUFFLING RECURRENT NEURAL NETWORKS

Michael Rotman
Tel Aviv University

Lior Wolf
Facebook AI Research and Tel Aviv University

ABSTRACT

We propose a novel recurrent neural network model, where the hidden state h_t is obtained by permuting the vector elements of the previous hidden state h_{t-1} and adding the output of a learned function $b(x_t)$ of the input x_t at time t . In our model, the prediction is given by a second learned function, which is applied to the hidden state $s(h_t)$. The method is easy to implement, extremely efficient, and does not suffer from vanishing nor exploding gradients. In an extensive set of experiments, the method shows competitive results, in comparison to the leading literature baselines.

1 Introduction

Recurrent Neural Networks (RNN) architectures have been successful in solving sequential or time dependent problems. Such methods maintain a latent representation, commonly referred to as the “hidden state”, and apply the same learned functions repeatedly to the input at each time step, as well as to the current hidden state.

A well-known challenge with RNNs, is that of exploding or vanishing gradients. The various methods that were devised in order to solve this problem can be roughly divided into two groups. The first group utilizes a gating mechanism to stabilize the gradient flow between subsequent hidden states [9, 4], whereas the second group focuses on preserving the norm of the hidden states by employing constraints on the family of matrices used as the network’s parameters [1, 8].

An alternative view of the problem of exploding and vanishing gradient considers it as the symptom of a deeper issue and not as the root cause. Current RNN architectures perform a matrix multiplication operation, with learned weights, over previously seen hidden states during each time step. Therefore, inputs appearing in different times are processed using different powers of the weight matrices (with interleaving non-linearities): the first input of a sequence of length T is processed by the same learned sub-network T times, whereas the last input at time T is processed only once. This creates an inherent gap in the way that each time step influences the network weights during training.

In this work, we propose an alternative RNN framework. Instead of using a learned set of parameters to determine the transition between subsequent hidden states, our method uses a parameter-free shift mechanism, in order to distinguish between inputs fed at different times. This shift mechanism forms an orthogonal matrix operation, and is, therefore, not prone to the gradient explosion or to its vanishing. Furthermore, the various time steps are treated in a uniform manner, leading to an efficient and perhaps more balanced solution. This allows us, for example, to learn problems with much larger sequence lengths than reported in the literature.

Our experiments show that our Shuffling Recurrent Neural Network (SRNN) is indeed able to tackle long-term memorization tasks successfully, and shows competitive results, in comparison to the current state of the art of multiple tasks. SRNN is elegant, easy to implement, efficient, and insensitive to its hyperparameters. We share our implementation at <https://github.com/rotmanmi/SRNN>.

2 Background and Related Work

RNNs have been the architecture of choice, when solving sequential tasks. The most basic structure, which we refer to as the vanilla RNN, updates at each time a hidden state vector h_t using an input x_t ,

$$h_t = \sigma(W_1 h_{t-1} + W_2 x_t) \equiv \sigma(z_t), \quad (1)$$

where σ is a non-linear activation function, such as \tanh or ReLU . Given a sequence of length T , $\{x_t\}_{t=1}^T$, computing the gradients of a loss function, \mathcal{L} , w.r.t to W_1 , $\frac{\partial \mathcal{L}}{\partial W_1}$, requires the application of the chain rule throughout all the hidden states $\{h_t\}_{t=1}^T$,

$$\frac{\partial \mathcal{L}}{\partial W_1} = \sum_{t=1}^T \frac{\partial \mathcal{L}}{\partial h_t} \frac{\partial h_t}{\partial W_1} = \sum_{t=1}^T \frac{\partial \mathcal{L}}{\partial h_t} \sigma'(z_t) h_{t-1}, \quad (2)$$

where $\frac{\partial \mathcal{L}}{\partial h_t} = \sum_{t'=t+1}^T \frac{\partial \mathcal{L}}{\partial h_{t'}} \frac{\partial h_{t'}}{\partial h_t}$ and $\frac{\partial h_{t'}}{\partial h_t} = \prod_{i=t}^{t'} \frac{\partial h_{i+1}}{\partial h_i} = \prod_{i=t}^{t'} \sigma'(z_i) W_1$. Depending on the maximal eigenvalue of W_1 , the repeated multiplication by W_1 in $\frac{\partial \mathcal{L}}{\partial h_t}$ may lead to exponential growth or decay in the gradients of $\frac{\partial \mathcal{L}}{\partial W_1}$ when $T \gg 1$.

Many of the successful RNN methods utilize a gating mechanism, where the hidden state h_t can be either suppressed or scaled, depending on a function of the previous hidden state and the input. Among these solutions, there is the seminal Long-Short Term Memory network (LSTM) [9] that utilizes a gating mechanism together with a memory cell, the powerful Gated Recurrent Unit (GRU) [4], and the recent Non-Saturating Recurrent Unit (NRU) [3] that makes use of a non-saturating function, such as a ReLU , for the activation function. These units often make use of a gradient clipping scheme while training, since they contain no inherent mechanism to deal with exploding gradients over very long time sequences.

A second family of RNNs focuses on constraining the weight matrix W_1 of the RNN to be orthogonal or unitary. Unitary Recurrent Neural Networks (uRNN) [1] force a strict structure regime on the parameter matrices, thus modifying these matrices in a sub-manifold of unitary matrices. Noting that the method neglects some types of unitary matrices, the Full-Capacity Unitary Recurrent Neural Network [19], uses a weight parameterization that spans the complete set of unitary matrices, by constraining the gradient to reside on a Stiefel manifold. EUNN [10] employs a more efficient method in order to span this set. Another efficient approach to optimize in this space, which is based on the Householder reflections, was proposed in [17], and a Cayley transform parameterization was used in [7, 16]. The recent nnRNN [11] method parameterizes the transformations between the successive hidden states using both a normal matrix and a non-normal one, where the first is responsible for learning long-scale dynamics and the second adds to the expressibility of the model.

3 Method

The SRNN layer contains two hidden-state processing components, the learned network b that is comprised of fully connected layers, and a fixed permutation matrix W_p . At each time step, the layer, like other RNNs, receives two input signals: the hidden state of the previous time step, $h_{t-1} \in \mathbb{R}^{d_h}$, and the input at the current time step, $x_t \in \mathbb{R}^{d_i}$, where d_h and d_i are the dimensions of the hidden state and the input, respectively. The following computation takes place in the layer (we redefine the notation, disregarding the definitions of Sec. 2):

$$h_t = \sigma(W_p h_{t-1} + b(x_t)) \equiv \sigma(z_t), \quad (3)$$

where σ is the activation function (such as ReLU or \tanh), see Fig. 1(a). The permutation operator W_p reflects the time dependency, whereas b is agnostic to the ordering of the input. Without loss of generality, the permutation can be chosen as the shift operation that can be represented by the off-diagonal matrix

$$W_p = \begin{pmatrix} 0 & 1 & 0 & \dots & 0 \\ 0 & \dots & \dots & \dots & 0 \\ \vdots & \dots & \dots & \dots & \vdots \\ 0 & \dots & \dots & \dots & 1 \\ 1 & 0 & \dots & 0 & 0 \end{pmatrix}. \quad (4)$$

Network b employs a two-headed structure for a self-gating mechanism. The primary branch is composed of a MLP $f_r : \mathbb{R}^{d_i} \rightarrow \mathbb{R}^{d_h}$. The gating branch scales the output of b and contains a single affine layer with a sigmoid activation function.

$$b(x_t) = f_r(x_t) \odot \text{sigmoid}(W_s x_t + b_s), \quad (5)$$

where $W_s \in \mathbb{R}^{d_h \times d_i}$ and $b_s \in \mathbb{R}^{d_h}$ are the weights and biases of the gating branch. Fig. 1(b) depicts the structure of network b .

The output of the network at time step t , o_t , is obtained by using a single affine layer s ,

$$o_t = s(h_t). \quad (6)$$

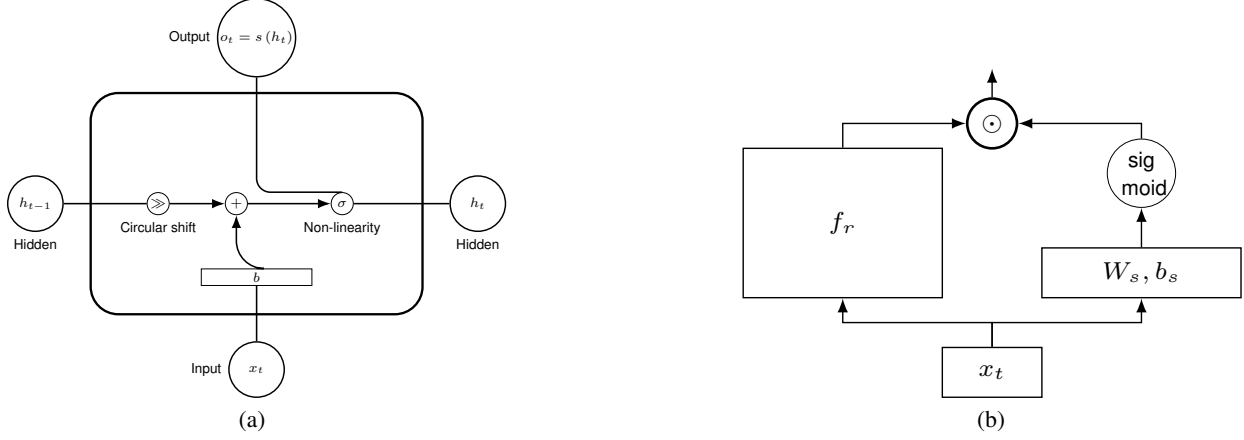


Figure 1: (a) The architecture of the SRNN layer. The output of b is added to the shifted version of the previous hidden state, followed by a non-linearity, σ . The output at time t is obtained by a function s that is applied to the new hidden state. (b) The structure of network b . The primary sub-network f_r is an MLP, the gating sub-network (right branch) has a single affine layer and a sigmoid non-linearity. The outputs of the two branches are multiplied elementwise to produce b 's output.

Analysis of gradient dynamics Since W_p is a permutation matrix, it is also orthogonal. Our method benefits from this property, since the successive applications of W_p do not increase nor decrease the norm of the hidden state vector, such that the gradients with respect to the hidden state do not suffer from an exponential growth or decay. Therefore, the method can be applied without the use of any gradient clipping schemes.

In addition, since the operator W_p is not learned, and the weights of network b do not appear with powers greater than one in the gradient. The gradient of the loss w.r.t a parameter b_k in network b is

$$\frac{\partial \mathcal{L}}{\partial b_k} = \sum_{t=1}^T \frac{\partial \mathcal{L}}{\partial h_t} \frac{\partial h_t}{\partial b_k}. \quad (7)$$

The derivative of Eq. 3 w.r.t b_k yields a recursive equation,

$$\frac{\partial h_t}{\partial b_k} = W_p \sigma'(z_t) \frac{\partial h_{t-1}}{\partial b_k} + \sigma'(z_t) \frac{\partial b(x_t)}{\partial b_k}. \quad (8)$$

Expanding Eq. 8 yields the closed form,

$$\frac{\partial h_t}{\partial b_k} = \sum_{i=1}^t \sigma'(z_i) \left(\prod_{j=1}^{i-1} [W_p \sigma'(z_j)] \right) \frac{\partial b(x_i)}{\partial b_k}. \quad (9)$$

Since W_p is orthogonal, the only terms that may influence the gradients' growth or decay are $\sigma'(z_t)$. For most used activation functions, such as the sigmoid, tanh and ReLU, $|\sigma'(z_i)|$ is bounded by 1. Therefore, one obtains

$$\left| \frac{\partial h_t}{\partial b_k} \right| \leq \left| \sum_{i=1}^t \frac{\partial b(x_i)}{\partial b_k} \right|. \quad (10)$$

Combining this result with Eq. 7 reveals that

$$\left| \frac{\partial \mathcal{L}}{\partial b_k} \right| \leq \left| \sum_{t=1}^T \frac{\partial \mathcal{L}}{\partial h_t} \sum_{i=1}^t \frac{\partial b(x_i)}{\partial b_k} \right|. \quad (11)$$

As $\frac{\partial \mathcal{L}}{\partial b_k}$ gains only linear contributions from the derivatives of b it cannot explode.

For the ReLU activation function, the gradients in Eq. 9 vanish if and only if there is some time t' in the future where $z_{t'} < 0$. Since previous hidden states can only increase h_t , negative contributions only arise due to the outputs of network b . These outputs, $b(x_t)$, approximately follow a normal distribution of $\mathcal{N}(0, 1)$ [6]. An estimation for the

Table 1: Time complexity for one gradient step for sequence length T . d_h, d_i =hidden state and input dims.

METHOD	TIME COMPLEXITY
VANILLA RNN	$O(Td_h^2 + Td_h d_i)$
GRU	$O(Td_h^2 + Td_h d_i)$
LSTM	$O(Td_h^2 + Td_h d_i)$
URNN	$O(Td_h \log d_h + Td_h d_i)$
NRU	$O(Td_h^2 + Td_h d_i)$
SRNN	$O(Td_h d_i)$

Table 2: Accuracy for the pMNIST and the bigger version, in which the MNIST image is embedded in a black image four times larger.

METHOD	PMNIST	BIG PMNIST
LSTM	89.50%	33.60%
GRU	91.87%	9.45%
URNN	91.74%	OUT OF MEMORY
NRU	91.64%	11.01%
SRNN	96.43%	90.31%

number of time steps it takes for a neuron in h_t to vanish is achieved by assuming that the probability of either obtaining a negative or a positive contribution to its activation at step t is $\frac{1}{2}$. This scenario is known as the Gambler’s Ruin problem [18]. Although the probability of having the hidden state vanish, $p(z_t \leq 0) = \frac{T}{1+T}$, approaches one for $T \gg 1$, the expectation value of the number of steps until this happens is T .

Time complexity The computation of h_t does not involve any matrix multiplications between previous hidden-state h_{t-1} , and the permutation operator can be applied in $O(d_h)$. The most time-consuming operator is the application of the function b . However, since b does not require any information from previous states, it can be applied in parallel to all time steps, thus greatly reducing the total runtime. The time complexity, in comparison to the literature methods, is presented in Table 1 for a minibatch of size one. It assumes that the number of hidden units in each layer of f_r is $O(d_i)$. As can be seen, our method is the only one that is linear in d_h .

4 Experiments

We compare our SRNN architecture to the leading RNN architectures from the current literature. The baseline methods include: (1) a vanilla RNN, (2) LSTM [9], (3) GRU [4], (4) uRNN [1], (5) NRU [3], and (6) nnRNN [11]. All methods, except NRU, employed the RMSProp [2] optimizer with a learning rate of 0.001 and a decay rate of 0.9. For NRU, we have used the suggested ADAM [12] optimizer with a learning rate of 0.001, and employed gradient clipping with a norm of one. The optimization parameters for nnRNN were taken from the official repository. For all problems involving one-hot inputs, we have added an embedding layer before the RNN, since it benefited all methods. We believe that reports, which have deemed GRU as ineffective in some of the proposed benchmarks, did not include such a layer. The activation function σ in Eq. 3 and within the network b was a ReLU. The activation function of the vanilla RNN (denoted ‘RNN’ in the figures) was tanh.

Copying Memory Problem RNNs are often challenged by the need to take into account information that has occurred in the distant past. The Copying Memory (MemCopy) task of [1] was designed to test the network’s ability to recall information seen in the past. The objective is to memorize the first 10 characters of the sequence. Let $A = \{a_i\}_{i=1}^8$ be a set of 8 symbols, a_9 the blank symbol and a_{10} , the delimiter symbol. we create a sequence with the length $T + 20$, where the first 10 symbols are taken from A , then the next $T - 1$ symbols are the blank symbol a_9 followed by a single appearance of the delimiter symbol, a_{10} . The last 10 symbols are again set to the blank symbol a_9 . The required output is a sequence of $T + 10$ blank symbols followed by the first 10 symbols taken from A of the original sequence. The baseline model for this task predicts some constant sequence after the appearance of the delimiter symbol, a_{10} . The cross-entropy for this solution is $\frac{10 \ln 8}{T+20}$.

We trained all models with a minibatch of size 20. We used a hidden size of $d_h = 128$ for all models. For f_r inside of the b function of the SRNN we have used one hidden layer of size 8, i.e., f_r projects the input to activations in \mathbb{R}^8 and then to \mathbb{R}^{128} .

Fig. 2 shows the cross-entropy loss for all models for the time lag of $T = 100, 200, 300, 500, 1000, 2000$. While most methods are successful in dealing with sequences of length $T = 100$, only the SRNN is able to deal efficiently with longer time lags. In contrast to results reported in the literature, the GRU and LSTM are able to partially solve this problem, and they even do so better than uRNN for sequences larger than 1000, where it starts to lose some of its stability. However, the convergence rate of LSTM and GRU is very slow. Note that the cross entropy obtained for SRNN, while better than other methods, can go up as training progresses. This is similar to what is observed in [1], for their uRNN method, in the cases where uRNN is successful. nnRNN is successful for $T \leq 300$ and is unstable for longer sequences.

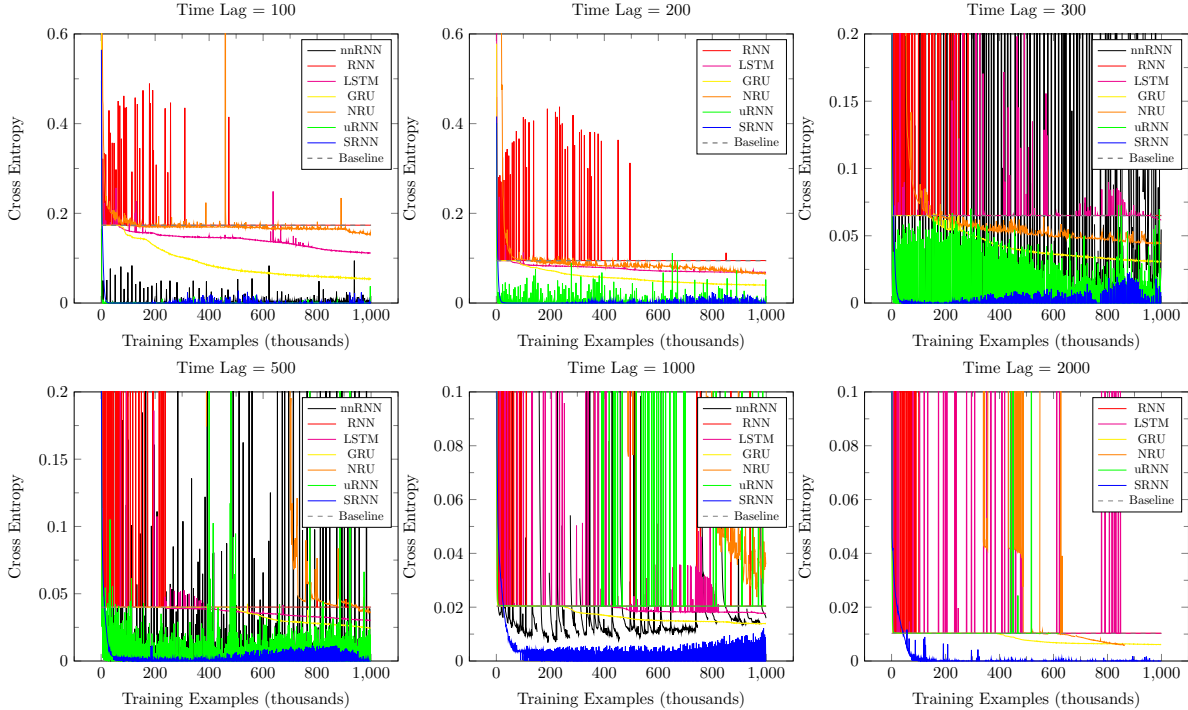


Figure 2: Results for the MemCopy task. Shown is the cross entropy as a function of the number of training examples. Each plot depicted the results for a different sequence length.

Adding Problem The adding problem was first introduced in [9]; We follow a close variant formulated in [1]. The input for this task consists of two sequences of length T (the two are concatenated to form x_t). The first sequence contains real numbers that have been uniformly sampled from $\mathcal{U}(0, 1)$. The second sequence is an indicator sequence, that is set to 0, except for two random entries that are set to 1. One of these entries is located in the first half of the sequence and the other in the last half of the sequence. The objective of this task is to output the sum of the two numbers in the first sequence that correspond to the location of the 1s in the second. The baseline to this task is the model which predicts 1, no matter what the input sequences are. The expected mean squared error (MSE) for this case is 0.167. A hidden size of 128 was used for all methods. All models were fed with a minibatch of 50. As in the MemCopy problem, all the training samples were generated on the fly. Network b of SRNN contains a hidden layer with size 8.

Fig. 3 shows the MSE for all models for sequence lengths of $T = 100, 200, 400, 750, 1000, 1500$. NRU, GRU and SRNN solve this problem quickly, with NRU showing very fast convergence. LSTM is also successful in solving this task, but its convergence is much slower. nnRNN is able to solve this task whenever it was able to initialize properly for sequence sizes shorter than 200.

Permuted Sequential MNIST The permuted MNIST (pMNIST) benchmark by [13] measures the performance of RNNs, when modeling complex long-term dependencies. In this task, each MNIST image is reshaped into a 784-dimensional vector. This vector is fed to the RNN one entry at a time. The objective is to classify the image at the last time step. In order to increase the difficulty of the problem, a fixed permutation matrix is applied on each of the vectors before feeding them to the neural network. The same permutation and samples were used to train and evaluate all methods.

In this task, all models had the order of 165k parameters, except for SRNN that had 50k parameters. We tried to initialize nnRNN with the same initialization presented in the literature of 800k parameters. However, it failed, so it was trained with less. Unfortunately, we were not able to get the vanilla RNN to converge on this task and nnRNN initialization (which depends on a numerical solver) failed, despite multiple efforts done using the official code of this method.

For SRNN, a hidden size of $d_h = 1024$ was used, and the function f_r of network b contained three hidden layers of size 32. A minibatch size of 100 was used for training, similar to the experiments performed by NRU. Models were trained for 60 epochs. Table 2 presents the accuracy over the test set for the epoch with the lowest cross entropy over the

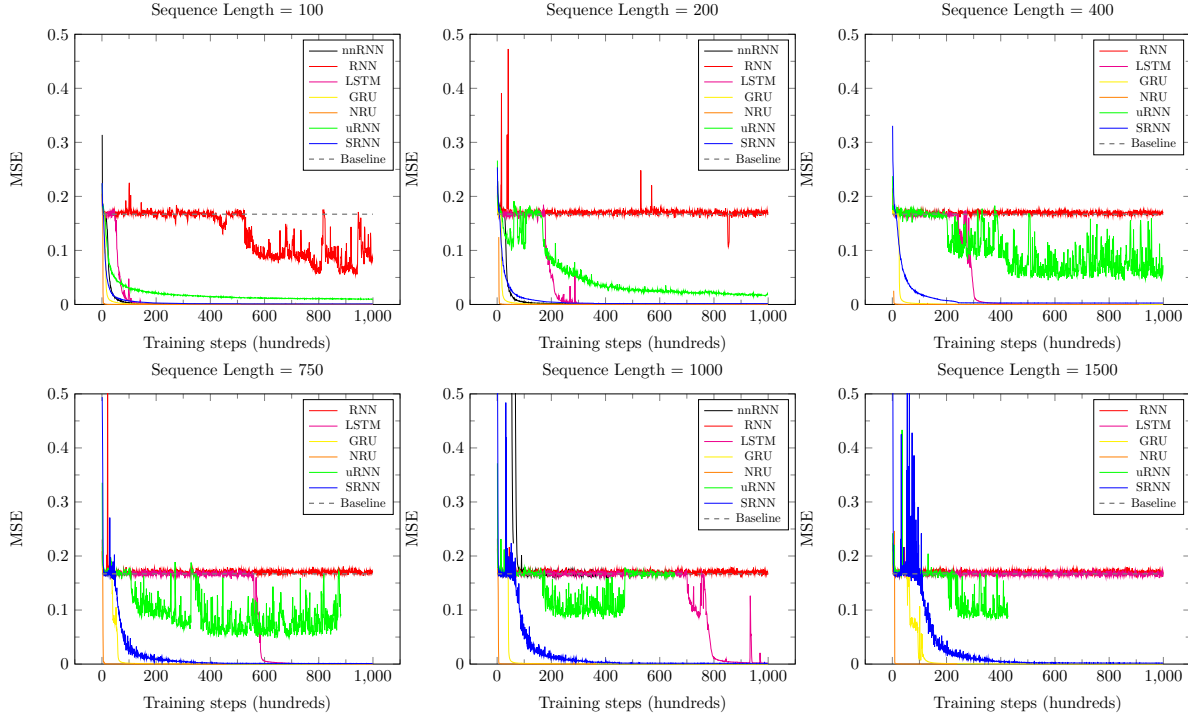


Figure 3: Results for the adding problem for varying sequence lengths, noted on the top of each plot. Shown are MSE as a function of the number of training steps for our method and the baseline methods. For a longer sequence length, we sometimes stopped the run of uRNN before the allocated number of training iterations, due to the slow runtime of this method.

Table 3: MSE on the TIMIT for various algorithms. d_h is the size of the hidden state. Src=source.

SRC METHOD	d_h	MSE	SRC METHOD	d_h	MSE	SRC METHOD	d_h	MSE		
LSTM	84	14.30	[14]	RGD	128	14.58	OUR RUNS	URNN	128	12.09
LSTM	120	12.95		RGD	128	14.58		URNN	256	10.83
LSTM	158	12.62		RGD	192	14.50		URNN	512	11.90
EXPRNN	224	5.30		RGD	256	14.69		NRU	128	12.26
EXPRNN	322	4.38	OUR RUNS	LSTM	128	19.78		NRU	256	5.90
EXPRNN	425	5.48		LSTM	256	15.91		NRU	512	3.23
SCORNN	224	8.50		LSTM	512	12.32		NRU	1024	0.35
SCORNN	322	7.82		LSTM	1024	8.66		SRNN	128	12.69
SCORNN	425	7.36		GRU	128	39.66		SRNN	256	7.85
EURNN	158	18.51		GRU	256	37.17		SRNN	512	4.73
EURNN	256	15.31	GRU	512	33.00	SRNN	1024	1.34		
EURNN	378	15.15	GRU	1024	26.53	SRNN	2048	0.64		

validation set. As can be seen, SRNN is more effective than all other methods. We cannot compare with IndRNN [15], which uses a different split.

In order to verify that our method is not overly sensitive to its parameters, namely the dimensionality of the hidden state and the depth and number of hidden units per layer of network f_r (the primary sub-network of b), we tested multiple configurations. The results are reported in Fig. 4(a) and show that the method’s accuracy is stable with respect to its parameters. As an ablation, we also report results in which gating is not used (the effect on the number of parameters is negligible). Without gating, performance somewhat decreases, especially for larger networks. However, overall, gating does not seem to be the most crucial part of the architecture.

Another version of pMNIST was tested, in which the MNIST image is padded with zeros, so that it is four times as large. The results are also reported in Table 2. Evidently, our method has an advantage in this dataset, which requires a

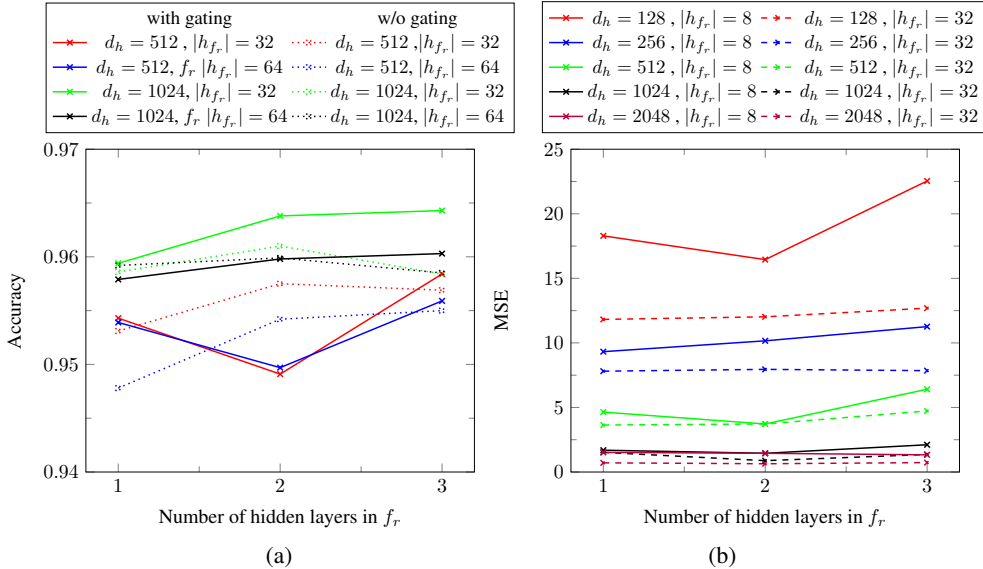


Figure 4: (a) SRNN accuracy on pMNIST for multiple configurations. For each configuration, we report the accuracy for up to three hidden layers. Dashed lines employ no gating in network b . (b) Same for TIMIT, reporting MSE, for varying d_h or the hidden state of f_r in b .

Table 4: The runtime in seconds for one training epoch for various methods on a minibatch of 100. For MemCopy and Adding $T = 300$, SRNN’s b network contains one hidden layer in f_r with 32 units. The number of samples in MemCopy epoch is 1000, and the number of samples in Adding epoch is 10000. In all cases $d_h = 128$. The same machine was used for all experiments.

	RUNTIME PER DATASET (SEC)				PARAM ADD	RUNTIME PER DATASET (SEC)				PARAM ADD	
	MEMCPY	ADD	pMNIST	TIMIT		MEMCPY	ADD	pMNIST	TIMIT		
RNN	0.18	1.53	19.64	1.76	17K	NRU	7.13	61.77	835.47	42.98	102K
LSTM	0.26	1.76	22.88	1.80	67K	uRNN	13.48	112.78	1510.54	76.10	2k
GRU	0.19	1.63	17.43	1.78	50K	SRNN	0.07	0.77	8.59	1.27	5K

much larger amount of memorization. Note that uRNN could not run due to GPU memory limitations, despite an effort to optimize the published code using TorchScript (<https://pytorch.org/docs/stable/jit.html>).

TIMIT The TIMIT [5] speech frames prediction task was introduced by [19] and later (following a fix to the way the error is computed) used in [14]. The train / validation/ test splits and exactly the same data used by previous work are employed here: using 3640 utterances for the training set, 192 for the validation set, and a test set of size 400.

Table 3 reports the results of various methods, while varying the dimensionality of the hidden state, both for our runs, and for baselines obtained from [14]. Despite some effort, we were not able to have the published code of nnRNN run on this dataset (failed initialization). Running uRNN for dimensionality larger than 512 was not feasible. As can be seen, our SRNN outperforms almost all of the baseline methods, including EXPRNN [14], SCORNN [7], EURNN [10], and RGD [19]. The only method that outperforms SRNN is NRU. However, the NRU architecture has an order of magnitude more parameters than our method for a given hidden state size; NRU with $d_h = 1024$ has more than ten times the number of parameters than SRNN with $d_h = 2048$.

The SRNN model used on TIMIT has three hidden layers in f_r , each with 32 hidden neurons in each. However, the method is largely insensitive to these parameters, as can be seen in Fig. 4(b). Networks with 8 hidden neurons in each layer perform slightly worse than those with 32, and the number of layers has a small effect when the dimensionality of the hidden state is high enough.

Visualization of the hidden units Fig. 5 provides a visualization of the hidden state, h_t of the SRNN for the Adding problem and the pMNIST task. For better visualization, the plot has been modified so the shift is removed. As can be seen, the method can retain information in cases in which memorization is needed, such as in the Adding problem. It also has the capacity to perform non-trivial computations in cases in which processing is needed, such as the pMNIST. SRNN also does not suffer from the vanishing gradient problem, since the activations are maintained over time.

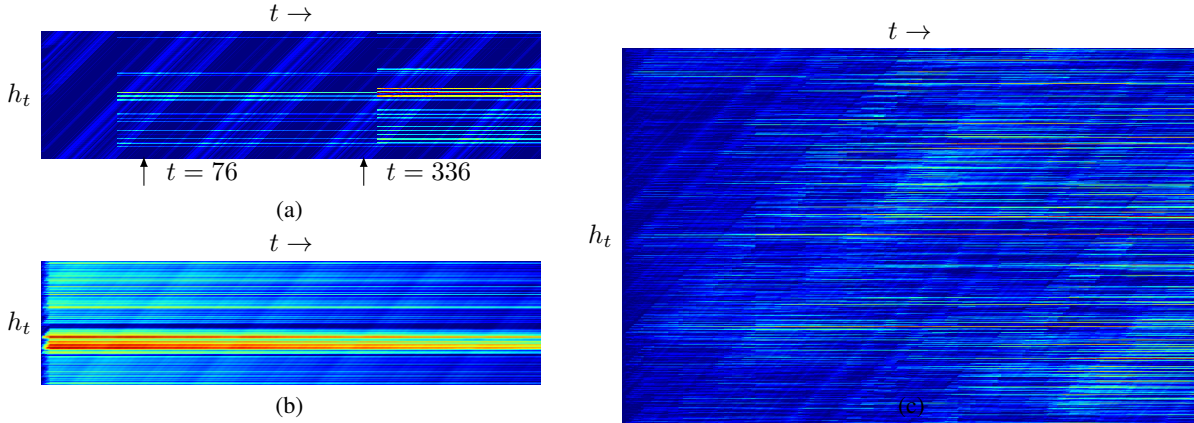


Figure 5: (a) The shifted hidden state of the SRNN for the Adding task. The arrows indicate the positions where the indicator sequence in x_t is set to 1. These positions split the hidden state into three regions. (b) The shifted hidden state of the SRNN for the MemCopy task. After $T = 10$ there is almost no change to the hidden state, as expected. (c) The shifted hidden state of the SRNN for the pMNIST task. Unlike the Adding or the MemCopy Task, the hidden state evolves through time, and the cell is able to suppress activations or accumulate additional information.

Fig. 6 provides a visualization of the hidden state, h_t of the SRNN for TIMIT. In this example h_t contains 2048 units. SRNN is able to remove irrelevant information for the future from the hidden state, an ability that is not required for the addition or the Memory Copy Tasks.

Capacity Since the orthogonal matrix SRNN employs is fixed, one may wonder if it is less expressive than other RNNs, or if it has less capacity. The experiments below indicate that the capacity of SRNN is comparable to that of other methods with the same number of hidden units (although by avoiding the usage of complex cells, the number of parameters is smaller).

One way to measure the SRNN capacity is to measure its ability to differentiate between samples taken from the same probability distribution. In order to create an artificial differentiation, all the labels of MNIST are shuffled, and then a subset of N samples is randomly selected. Since the focus of this experiment is not assessing the ability of the SRNN or other baseline models to tackle long sequences, the MNIST images are cropped to a 8×8 or 16×16 center patches, so the generated sequences are now 64 or 256 steps long. For this experiment the models were selected to have an order of $15K$ parameters. Testing is done on the training samples, since the aim is to measure the ability overfit random labels.

Fig. 7 presents the classification accuracy with respect to the random label for the SRNN, LSTM, GRU and the vanilla RNN architectures for different subset sizes, $N = 100, 1000, 10000$ and cropped patches of size 8×8 . As can be seen, for $N = 100, 1000$, all models are able to differentiate between the different samples, i.e., overfit to the random labels. For the case of $N = 10000$, all models succeed, except for the vanilla RNN.

Fig. 8 depicts a similar experiment for the case of 16×16 patches. For $N = 100$ and $N = 1000$ all methods are able to overfit, however, SRNN shows a marked advantage in the number of required training epochs. For $N = 10,000$, only SRNN and GRU are able (partially) overfit the data.

In addition, it is evident (in both settings) that as the sequence length increases, SRNN fits the data faster, which suggests that it has a high capacity and/or that it trains more effectively.

Runtime Table 4 compares the runtime of our method, for a single epoch on each listed dataset, in comparison to the official implementations of other methods. As can be seen, our method is much more efficient than the other methods. In the same set of experiments, we also recorded the number of parameters reported by pytorch. This number is the same across benchmarks, except for the embedding size and the results reported are from the adding problem, where the embedding size is negligible. The only method with fewer parameters than our method is uRNN, which parameterizes the unitary transformation very efficiently.

5 Conclusions

In this work, we introduce a new RNN architecture that does not suffer from vanishing and exploding gradients. The method employs gating only on the sub-network that processes the input, makes use of a fixed shifting operator as an

orthogonal transformation of the hidden states, is efficient, and has a lower complexity than other RNN architectures. The new method obtains competitive results in comparison with previous methods, which rely on much more sophisticated machinery.

Acknowledgments

Tel Aviv University (TAU) has received funding for this project from the European Research Council (ERC) under the European Unions Horizon 2020 research and innovation program (grant ERC CoG 725974). The authors would like to thank Amit Dekel for valuable insights and Daniel Dubinsky for the CUDA-optimized implementation. The contribution of the first author is part of a Ph.D. thesis research conducted at TAU.

References

- [1] Martin Arjovsky, Amar Shah, and Yoshua Bengio. Unitary evolution recurrent neural networks. In *Proceedings of the 33rd International Conference on International Conference on Machine Learning - Volume 48*, ICML'16, page 1120–1128. JMLR.org, 2016.
- [2] Yoshua Bengio. Rmsprop and equilibrated adaptive learning rates for nonconvex optimization. *corr abs/1502.04390*, 2015.
- [3] Sarath Chandar, Chinnadhurai Sankar, Eugene Vorontsov, Samira Ebrahimi Kahou, and Yoshua Bengio. Towards non-saturating recurrent units for modelling long-term dependencies. In *Proceedings of the AAAI Conference on Artificial Intelligence*, volume 33, pages 3280–3287, 2019.
- [4] Kyunghyun Cho, Bart van Merriënboer, Caglar Gulcehre, Dzmitry Bahdanau, Fethi Bougares, Holger Schwenk, and Yoshua Bengio. Learning phrase representations using RNN encoder–decoder for statistical machine translation. In *Proceedings of the 2014 Conference on Empirical Methods in Natural Language Processing (EMNLP)*, pages 1724–1734, Doha, Qatar, October 2014. Association for Computational Linguistics.
- [5] John S Garofolo, Lori F Lamel, William M Fisher, Jonathan G Fiscus, and David S Pallett. Darpa timit acoustic-phonetic continuous speech corpus cd-rom. nist speech disc 1-1.1. *NASA STI/Recon technical report n*, 93, 1993.
- [6] Kaiming He, Xiangyu Zhang, Shaoqing Ren, and Jian Sun. Delving deep into rectifiers: Surpassing human-level performance on imagenet classification. In *Proceedings of the IEEE international conference on computer vision*, pages 1026–1034, 2015.
- [7] Kyle Helfrich, Devin Willmott, and Qiang Ye. Orthogonal recurrent neural networks with scaled cayley transform. In *International Conference on Machine Learning*, pages 1969–1978, 2018.
- [8] Mikael Henaff, Arthur Szlam, and Yann LeCun. Orthogonal rnns and long-memory tasks. *CoRR*, abs/1602.06662, 2016.
- [9] Sepp Hochreiter and Jürgen Schmidhuber. Long short-term memory. *Neural Comput.*, 9(8):1735–1780, November 1997.
- [10] Li Jing, Yichen Shen, Tena Dubcek, John Peurifoy, Scott Skirlo, Yann LeCun, Max Tegmark, and Marin Soljačić. Tunable efficient unitary neural networks (eunn) and their application to rnns. In *Proceedings of the 34th International Conference on Machine Learning-Volume 70*, pages 1733–1741. JMLR. org, 2017.
- [11] Giancarlo Kerg, Kyle Goyette, Maximilian Puelma Touzel, Gauthier Gidel, Eugene Vorontsov, Yoshua Bengio, and Guillaume Lajoie. Non-normal recurrent neural network (nnrnn): learning long time dependencies while improving expressivity with transient dynamics. In *Advances in Neural Information Processing Systems*, pages 13591–13601, 2019.
- [12] Diederik P Kingma and Jimmy Ba. Adam: A method for stochastic optimization. *arXiv preprint arXiv:1412.6980*, 2014.
- [13] Quoc V Le, Navdeep Jaitly, and Geoffrey E Hinton. A simple way to initialize recurrent networks of rectified linear units. *arXiv preprint arXiv:1504.00941*, 2015.
- [14] Mario Lezcano-Casado and David Martínez-Rubio. Cheap orthogonal constraints in neural networks: A simple parametrization of the orthogonal and unitary group. In *International Conference on Machine Learning*, pages 3794–3803, 2019.
- [15] Shuai Li, Wanqing Li, Chris Cook, Ce Zhu, and Yanbo Gao. Independently recurrent neural network (indrnn): Building a longer and deeper rnn. In *Proceedings of the IEEE conference on computer vision and pattern recognition*, pages 5457–5466, 2018.

- [16] Kehelwala DG Maduranga, Kyle E Helfrich, and Qiang Ye. Complex unitary recurrent neural networks using scaled cayley transform. In *Proceedings of the AAAI Conference on Artificial Intelligence*, volume 33, pages 4528–4535, 2019.
- [17] Zakaria Mhammedi, Andrew Hellicar, Ashfaque Rahman, and James Bailey. Efficient orthogonal parametrisation of recurrent neural networks using householder reflections. In *Proceedings of the 34th International Conference on Machine Learning-Volume 70*, pages 2401–2409. JMLR. org, 2017.
- [18] J Michael Steele. *Stochastic calculus and financial applications*, volume 45. Springer Science & Business Media, 2012.
- [19] Scott Wisdom, Thomas Powers, John R. Hershey, Jonathan Le Roux, and Les Atlas. Full-capacity unitary recurrent neural networks. In *Proceedings of the 30th International Conference on Neural Information Processing Systems*, NIPS’16, page 4887–4895, Red Hook, NY, USA, 2016. Curran Associates Inc.

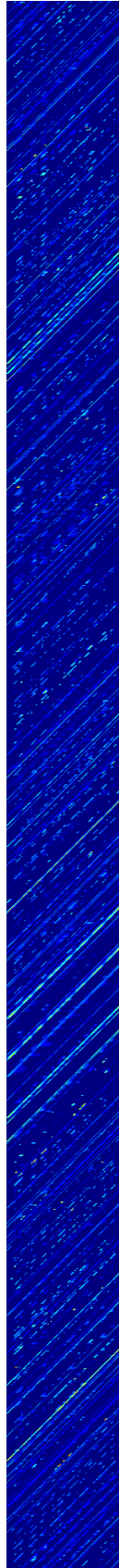


Figure 6: The shifted hidden state of the SRNN with 2048 units for the TIMIT task with a sequence length of $T = 151$.

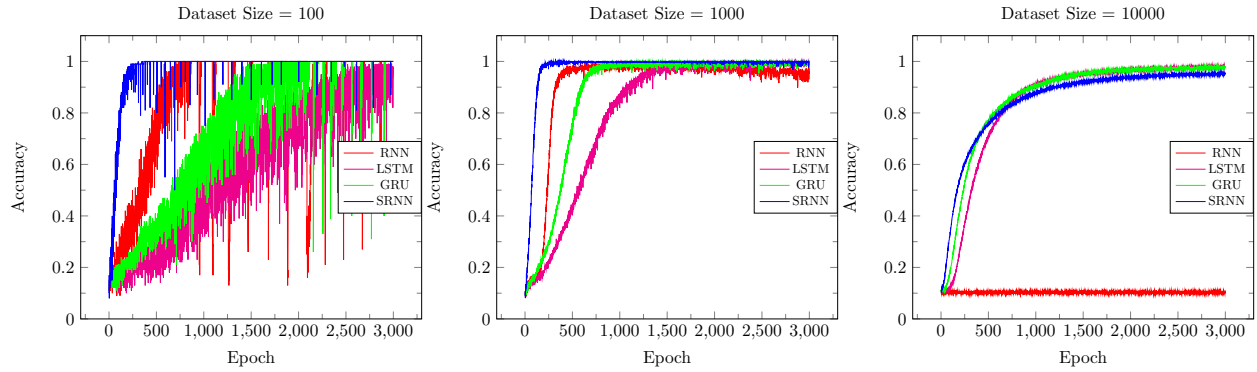


Figure 7: Fitting random labels for $N = 100, 1000, 10000$ samples of 8×8 cropped from MNIST images.

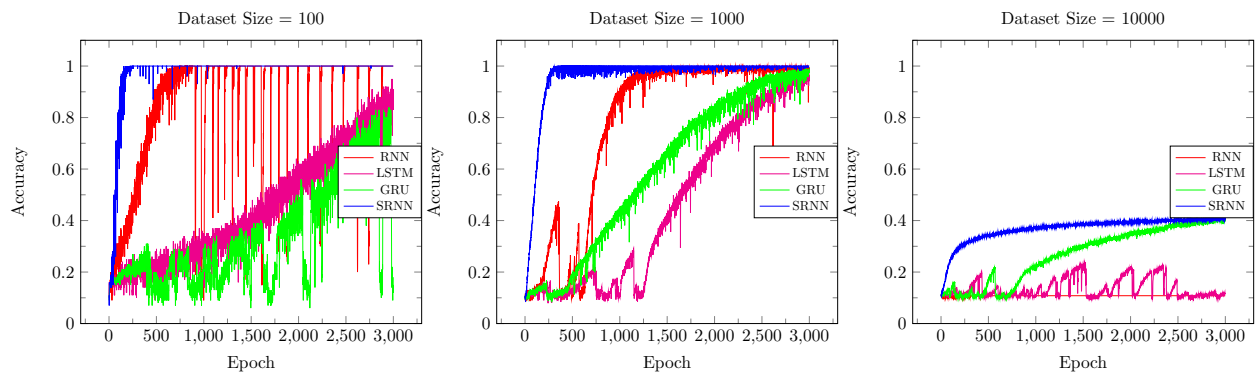


Figure 8: Fitting random labels for $N = 100, 1000, 10000$ samples of 16×16 cropped from MNIST images.